JOURNAL OF MATERIALS SCIENCE 28 (1993) 482–488

The characterization of plasma-sprayed/rapid omnidirectional compaction – processed tantalum coatings as applied to densified ceramic substrates

H. R. HERBOLSHEIMER, K. E. HOWARD*, R. A. NEWMAN
Central Research – Advanced Ceramics Laboratory, and Analytical Sciences Laboratory of The Dow Chemical Company, Midland, MI 48674, USA

The application of rapid omnidirectional compaction (ROC) processing to plasma-sprayed tantalum coatings in order to produce dense wear-resistant tantalum carbide coatings on a variety of predensified ceramic substrates is reported. Substrate materials included aluminium nitride, silicon carbide, silicon nitride, and WC–6Co. In particular, the phase chemistry which evolves during ROC processing, the surface morphology of the coating as-deposited and after ROC processing, and the erosive wear resistance of the coatings, are discussed.

1. Introduction

Plasma-spray deposition is a coating technique in which developments are occurring rapidly, in particular with respect to wear-, corrosion- and heat-resistant coatings (see, for example, [1]). A number of reviews have been published discussing the technical aspects of low-pressure plasma-spray (LPPS) deposition [2–5]. Hot isostatic pressing (HIPing) has been applied to the densification of, for example, WC–Co coatings for improved density, and adhesive and cohesive bonding of the coating [6]. Finally, the influence of plasma-sprayed ceramic coatings as applied to silicon carbide materials has recently been discussed [7]. The interaction of sputtered tantalum films with ceramic reinforcement materials has also recently been reported [8].

Rapid omnidirectional compaction (ROC) is a high-pressure (120×10^3 p.s.i., 0.8 GPa) process which has been applied to the densification of many metal, ceramic–metal, and ceramic materials [9]. We report here the application of ROC processing to plasma-sprayed tantalum coatings in order to produce dense wear-resistant tantalum carbide coatings on a variety of predensified ceramic substrates. Conversion of the as-deposited tantalum coating to tantalum carbide was performed during the ROC process preheat cycle. In particular, we have examined the phase chemistry which evolves during ROC processing, the surface morphology of the coating as-deposited and after ROC processing, and the erosive wear-resistance of the coatings.

2. Experimental procedure

2.1. Materials

Sintered aluminium nitride, hot-pressed self-reinforced silicon nitride [10], and sintered silicon carbide substrates were obtained from The Dow Chemical Company's Central Research and Development personnel. The tungsten carbide/cobalt substrates (WC–6%Co) were of a commercially available material (STB-824A, C-2 grade) obtained from Mahar Tool Company of Saginaw, Michigan. The tantalum powder used for the plasma-spray feed was Fansteel Tantalum Lot FC-21-558.

2.2. Plasma-spray deposition

Plasma-spray deposition was performed at the Plasma Laboratory of the Institute of Materials Processing, Michigan Technological University, using a low-pressure plasma-spray unit (Electro-Plasma, Inc., California) operating at a chamber pressure of 30 torr (1 torr = 133.322 Pa) and an Allen Bradley control unit. The primary gas used throughout the plasma-spray experiments was argon at 150 p.s.i.g. and a flow rate of 250 SCFH (standard cubic feet per hour) with a secondary gas of hydrogen (105 p.s.i.g., 32 SCFH). The secondary gas was incorporated to improve the enthalpy of the plasma and consequently improve the melting of the metal-feed powders. The powder-feed hopper was maintained at 40 p.s.i. with a gas flow of 13 SCFH and a powder feed rate of $\sim 6.8\,\mathrm{lb\,h^{-1}}$ ($51.6\,\mathrm{g\,min^{-1}}$). The feed hopper was rotated at a rate of 0.5 r.p.m. A stand-off distance of 12 in (~ 30.5 cm) between the plasma gun orifice and the substrate was used. Plasma operating conditions utilized 1500 A and 56 V.

Preliminary experiments frequently resulted in coatings which readily delaminated. This appeared to arise from overheating of the substrate. Reduction of the number of preheat cycles to one and increasing

* Author to whom all correspondence should be addressed.

0022–2461

the delay time between coating passes alleviated this problem. All coating passes were performed at the same robotic arm (which holds the plasma gun) velocity. One cycle refers to passing the plasma gun over the substrate to a predetermined position and returning to the origin. In this procedure one cycle lasted 2 s.

2.3. ROC processing conditions

Prior to ROC consolidation, all substrates were wrapped in a graphite foil to eliminate reaction with the pocket glass media and to provide a reactive carbon source for the conversion of the plasma-sprayed metal coatings to the corresponding carbides. ROC processing involved a 2 h preheat of the fluid die assembly to 1200 °C followed by compaction at a rate of 30 $\times 10^3$ p.s.i. s^{-1} to a maximum pressure of 120 $\times 10^3$ p.s.i. and a hold time of 30 s. After ROC processing the graphite outerwrap was removed prior to analysis.

2.4. X-ray diffraction and X-ray fluorescence analysis

X-ray diffraction data were collected in the Dow Analytical Sciences diffraction laboratory using a Siemens D-500 automated diffractometer, equipped with a CoK_{α_1} X-ray source and position-sensitive detector. The 2.5 cm × 7 cm plates were mounted directly in a custom-made adjustable diffractometer sample stage. The resulting diffraction spectra were subjected to a second derivative peak search to create a diffraction peak position and intensity (d and I) file for subsequent phase-identification analysis.

Elemental data were obtained by X-ray fluorescence and collected using a Tracor Northern TN-2000 energy dispersive X-ray fluorescence (EDXRF) analyser equipped with two sealed X-ray sources: an ^{55}Fe source and an ^{241}Am source with a molybdenum secondary target.

2.5. Optical microscopy

Optical photomicrographs of the as-sprayed and post-ROC processed samples, where the substrate was aluminium nitride or tungsten carbide/cobalt, were taken using a Nikon Epiphot™ optical microscope system. Photomicrographs were taken at a magnification of ×200 using a polarized light system.

2.6. Erosive wear testing

Erosion testing (following ASTM G65) was performed at Dow. The conditions for the testing were 30° angle of incidence, 30 min test duration, an average powder flow of 8.38 g min^{-1}, and a particle velocity of 227 ft s^{-1} ($\sim 6.92 \times 10^3$ cm s^{-1}). Erosion values reported reflect the volume loss of material in cubic millimetres per gram.

3. Results and discussion

3.1. Phase composition analysis of plasma-sprayed tantalum films on various substrates by X-ray powder diffraction

Phase-identification analysis by X-ray diffraction was performed on five samples. The samples were identified as described in Table I. The samples will be referred to by their labels, CUE1–CUE4NR. All of the samples except CUE4NR were processed using rapid omnidirectional compaction (ROC) after plasma-spray deposition of the tantalum coating. Sample CUE4NR was used to determine the identity of the tantalum phase(s) on these materials prior to ROC processing.

The principal tantalum phase as observed on the as-plasma-sprayed sample (CUE4NR) was $TaN_{0.1}$, JCPDS pattern 25-1278. All of the ROC-processed samples, CUE1–CUE4, exhibit a strong pattern corresponding to TaC, JCPDS 35-801. Detailed descriptions of the minor phases observed in each of the samples is given below.

3.1.1. Silicon nitride with tantalum (ROC-processed)

This sample exhibited both gold- and silver-coloured regions on the coated surface. The gold colour was believed to be due to TaC, therefore this region of the sample was analysed by X-ray diffraction. To determine what other elements were present, qualitative X-ray fluorescence (EDXRF) was performed on CUE1. This analysis indicated the following elements were present: tantalum, yttrium, strontium and calcium. Because EDXRF is qualitative, it was not possible to determine the amounts of these elements present in CUE1.

The following phases were identified by X-ray diffraction, listed in order of pattern intensity (the most intense pattern is listed first).

1. TaC, JCPDS 35-801.
2. $CaTa_4O_{11}$, JCPDS 15-679.
3. C, JCPDS 25-284 (graphite).
4. β-Si_3N_4, JCPDS 33-1160.
5. $SrTa_4O_{11}$ JCPDS 16-708.

The following diffraction lines were not assigned: 0.517, 0.464, 0.349, and 0.252 nm. Because the gold-

TABLE I Tantalum-coated samples used in this study

Sample	Material
CUE1	Hot-pressed Si_3N_4 with tantalum coating (ROC processed)
CUE2	Sintered AlN with tantalum coating (ROC processed)
CUE3	Sintered SiC with tantalum coating (ROC processed)
CUE4	WC–Co with tantalum coating (ROC processed)
CUE4NR	WC–Co with tantalum coating (as-sprayed)

coloured region of the surface was analysed, the graphite pattern was minor. The silver-coloured region of the sample was also analysed, and a very strong graphite pattern was observed. Thus, the silver colouration of CUE1 is due to the presence of graphite, which is used as the outerwrap for ROC-processing. Yttrium was identified as present in the sample (by EDXRF analysis). No yttrium phase was identified, but yttrium could substitute for both calcium and strontium in the ATa_4O_{11} phases (where A = Ca or Sr).

3.1.2. Aluminium nitride with tantalum (ROC-processed)

This sample also exhibited both gold- and silver-coloured regions on the tantalum-coated surface, but the gold-coloured region was much larger and more uniform than that observed for CUE1. The most uniform section of the gold-coloured region was analysed by both X-ray diffraction and qualitative X-ray fluorescence (EDXRF). The following elements were found to be present: tantalum, yttrium, calcium and strontium. No concentrations could be determined; however, the signals due to tantalum and yttrium were much stronger than the signal for calcium or strontium.

The following phases were identified by X-ray diffraction, listed in order of pattern intensity.

1. TaC, JCPDS 35-801.
2. AlN, JCPDS 25-1133.
3. $CaTa_2O_6$, JCPDS 36-805.
4. $AlTaO_4$, JCPDS 25-1490.
5. $CaTa_4O_{11}$, JCPDS 15-679.

The following diffraction lines were not assigned: 0.518, 0.345, 0.232, 0.215, and 0.190 nm. The graphite pattern observed from CUE2 was even weaker than that observed for CUE1. Although yttrium is a known additive to AlN as a sintering aid, no yttrium-containing phase was identified. As in the case of CUE1, yttrium could substitute for calcium in the Ca–Ta–O phases identified on the surface of CUE2.

3.1.3. Silicon carbide with tantalum (ROC-processed)

Again this sample exhibited both gold- and silver-coloured regions similar to CUE1. A circular area ~ 1 cm diameter, exhibited a relatively uniform gold colour, the remainder of the 2.5 cm × 7 cm surface was primarily silver. These two regions were analysed separately by X-ray diffraction, and were found to exhibit similar diffraction patterns with the exception of a very strong pattern due to graphite from the silver-coloured region, which is the source of the silver colour. Because it is used as an outerwrap, the graphite pattern is strong because it is coated on top of the gold-coloured TaC film, yielding the silver-coloured regions of Sample CUE3 as well as CUE1 and CUE2. EDXRF of CUE3 indicated the presence of the following elements: tantalum, silicon and calcium. The signal for calcium was relatively weak.

The following phases were identified by X-ray diffraction, listed in order of pattern intensity.

1. TaC, JCPDS 35-801.
2. C, JCPDS 25-284.

Several of the remaining lines fit the pattern of $CaTa_4O_{11}$ to some extent; however; this would have to be an oriented phase because some of the lines from the $CaTa_4O_{11}$ reference pattern are not observed in the pattern from CUE3 (see Fig. 1). Additionally, some of the lines which appear to "match" the $CaTa_4O_{11}$ pattern are shifted by differing amounts to lower *d*-spacing values. This type of variation is usually caused by substitution of a different element (for calcium in this case) into the lattice. From the observed X-ray pattern, it may be concluded that either $CaTa_4O_{11}$ or a structurally related phase is present in this sample.

Even after assuming that a $CaTa_4O_{11}$-type phase is present, many lines remain unidentified: 0.520, 0.467, 0.395, 0.391, 0.350, 0.345, 0.245, 0.239, 0.236, 0.232, 0.1964, 0.1858, 0.1780, 0.1757, 0.1744, 0.1636, 0.1468, 0.1451, 0.1269, 0.1259, 0.1243 nm. This residual pattern is indicated by ticks in Fig. 1.

3.1.4. Samples CUE4NR (WC–6Co with tantalum as-deposited) and CUE4 (WC–6Co with tantalum ROC-processed)

Sample CUE4NR was the only sample not ROC processed after plasma spraying. The sample was gold–grey in colour. Closer visual inspection revealed that the gold colour was present as small spots. After ROC processing (sample CUE4), two distinct regions were visible, a light-gold and a dark-gold region. The darker gold region was analysed by X-ray diffraction. Qualitative X-ray fluorescence of both samples indicated the presence of the following elements: tantalum and cobalt. Analysis for calcium could not be performed due to the large sample size of these substrates.

The following phases were identified in Sample CUE4NR by X-ray diffraction, listed in order of pattern intensity.

1. $TaN_{0.1}$, JCPDS 25-1278.
2. WC, JCPDS 25-1047.
3. W, JCPDS 4-806.

The following phases were identified in Sample CUE4 (post-ROC processed) by X-ray diffraction, listed in order of pattern intensity.

1. TaC, JCPDS 35-801.
2. WC, JCPDS 25-1047.
3. $CaTa_4O_{11}$ JCPDS 15-679.
4. C, JCPDS 25-284 (graphite).

Several of the remaining lines fit the reference pattern of $CaTa_4O_{11}$, but the pattern is oriented. Virtually all of the $CaTa_4O_{11}$ lines are observed, but some are much weaker than predicted by the JCPDS standard

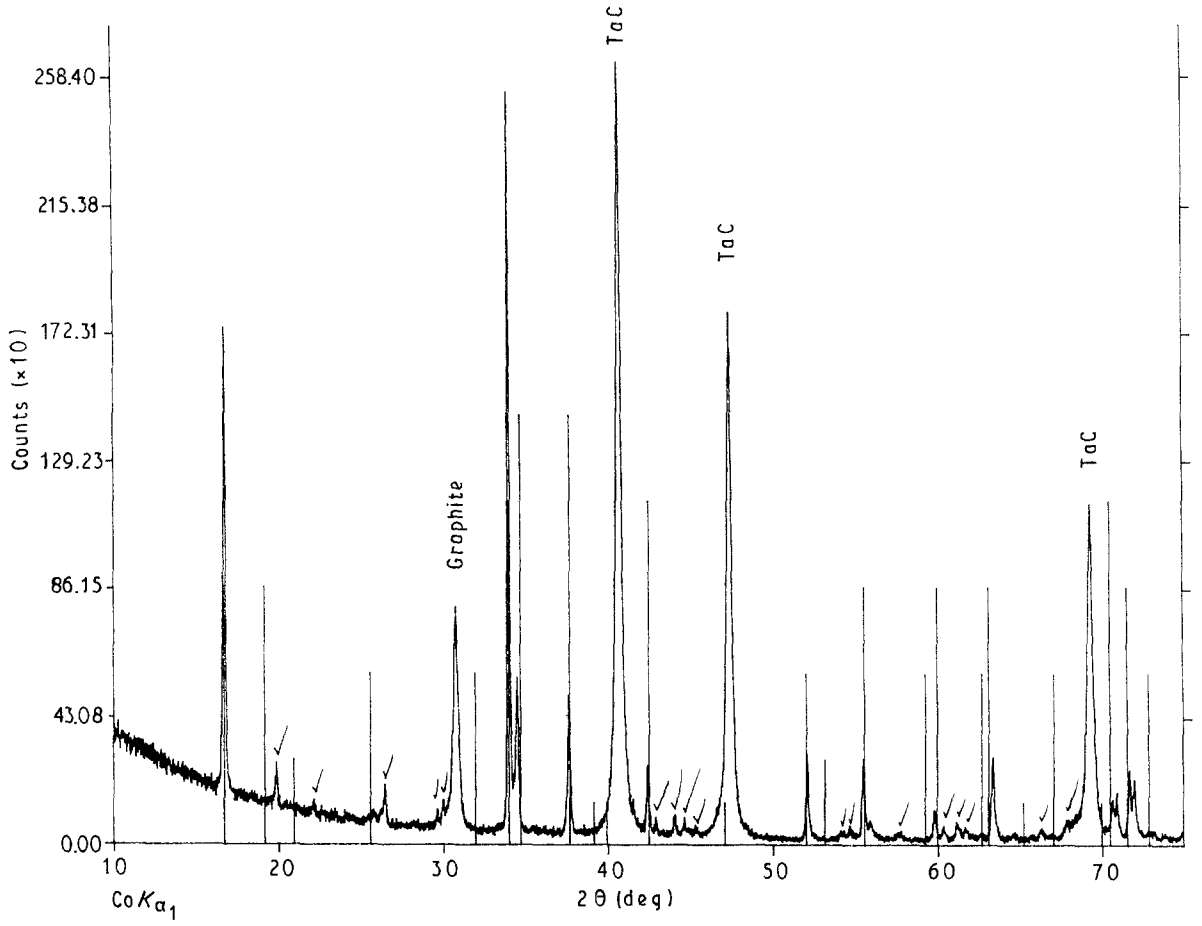

Figure 1 X-ray diffraction data from Sample CUE3. The stick spectrum is the standard diffraction pattern of $CaTa_4O_{11}$. Note the ticks, which indicate the unidentified residual pattern.

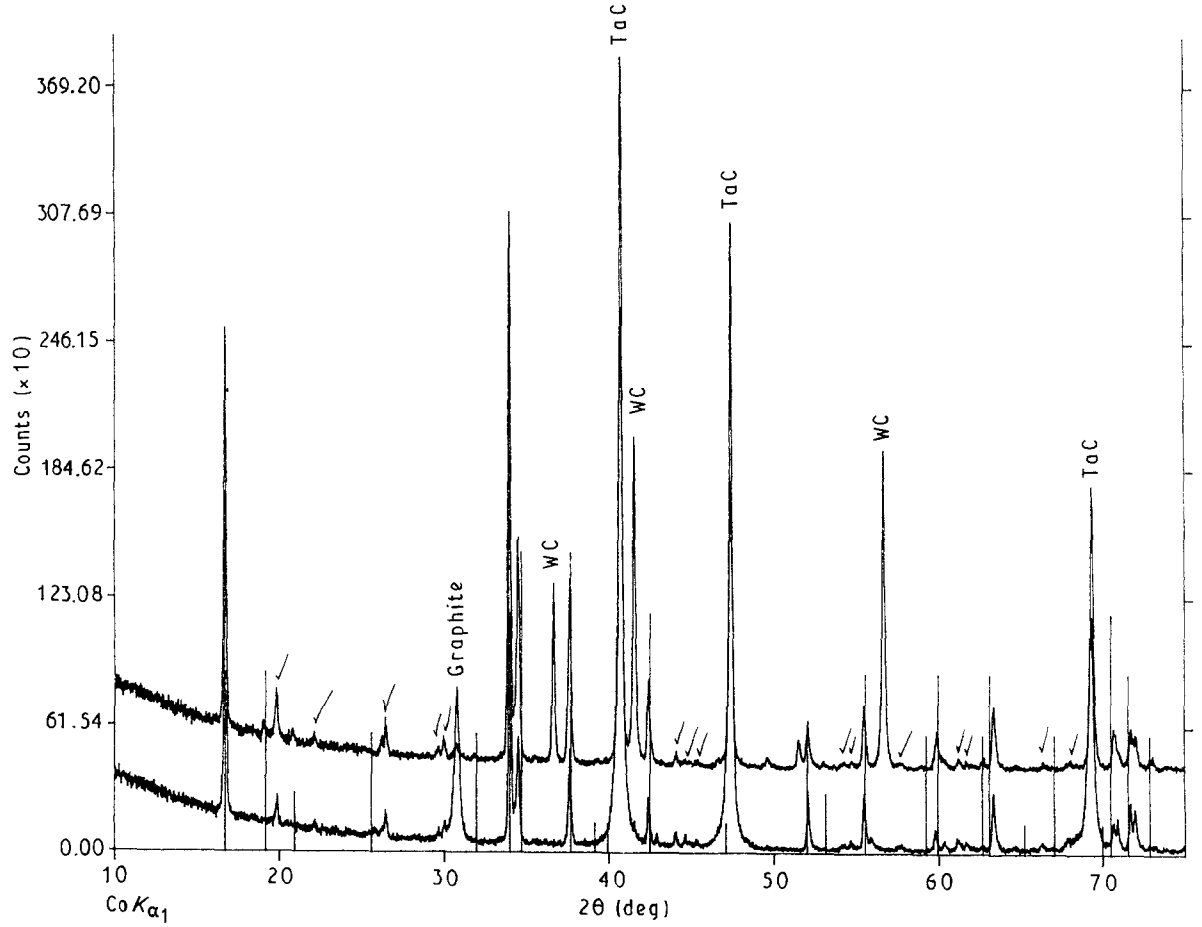

Figure 2 X-ray diffraction data from Samples CUE3 and CUE4 (upper). The stick spectrum is the standard diffraction pattern of $CaTa_4O_{11}$. The ticks indicate the unidentified residual pattern.

pattern. A comparison of the data from CUE4 with the data of CUE3 is shown in Fig. 2. Upon closer examination, it can be seen that the peaks for $CaTa_4O_{11}$ at ~ 19°, 32°, 53°, and 63° 2θ are present in the data from sample CUE4, but are *not* observed in the CUE3 sample data. From this comparison, it is clear that the orientation of the $CaTa_4O_{11}$-type phase is much greater for sample CUE3 than for CUE4. As in the case of CUE3, some of the lines which appear to "match" the $CaTa_4O_{11}$ pattern are shifted by differing amounts. The degree of line shift appears to be less than was observed for CUE3. Again, this type of variation is usually caused by substitution of a different element (for calcium in this case) into the lattice. Calcium has been observed as an impurity in WC/Co materials [11].

Many lines remain unidentified. This residual pattern is *virtually identical* to the residual pattern observed for sample CUE3, shown in Fig. 2.

3.1.5. Summary of X-ray diffraction results

The principal tantalum phase as observed on the as-plasma-sprayed sample (CUE4NR) is $TaN_{0.1}$, JCPDS pattern 25-1278. All of the ROC processed samples, CUE1–CUE4, exhibit a strong pattern corresponding to TaC, JCPDS 35-801. In all cases the deposited tantalum coatings (present generally as $TaN_{0.1}$) are converted to tantalum carbide, TaC, after ROC processing at 1200 °C. In addition, the presence of ATa_4O_{11} phases are observed in the post-ROC samples, suggesting that there is an interfacial reaction between the applied coating and sintering additives in the substrates.

3.2. Optical microscopy of as-sprayed and post-ROC processed coatings

Optical photomicrographs (× 200) of the as-sprayed and ROC-processed coatings are given in Figs 3 and 4. Despite the use of hydrogen as a secondary gas in the plasma-spray deposition process, in order to increase the enthalpy of the plasma flame and thereby increase the powder-melting efficiency, numerous unmelted or partially melted spheres were observed in the as-sprayed samples. In addition, the morphology of the as-sprayed coatings was coarse. In the ROC processed samples, however, the coatings appeared

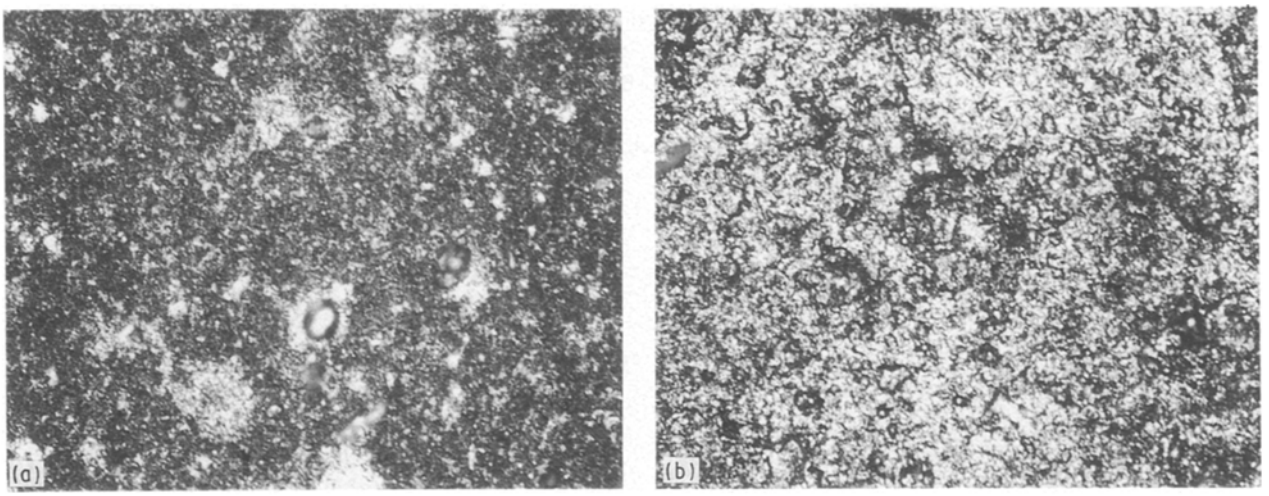

Figure 3 Optical photomicrograph of tantalum coating on aluminium nitride substrate, × 200. (a) As-plasma-sprayed tantalum coating. (b) ROC processed at 1200 °C.

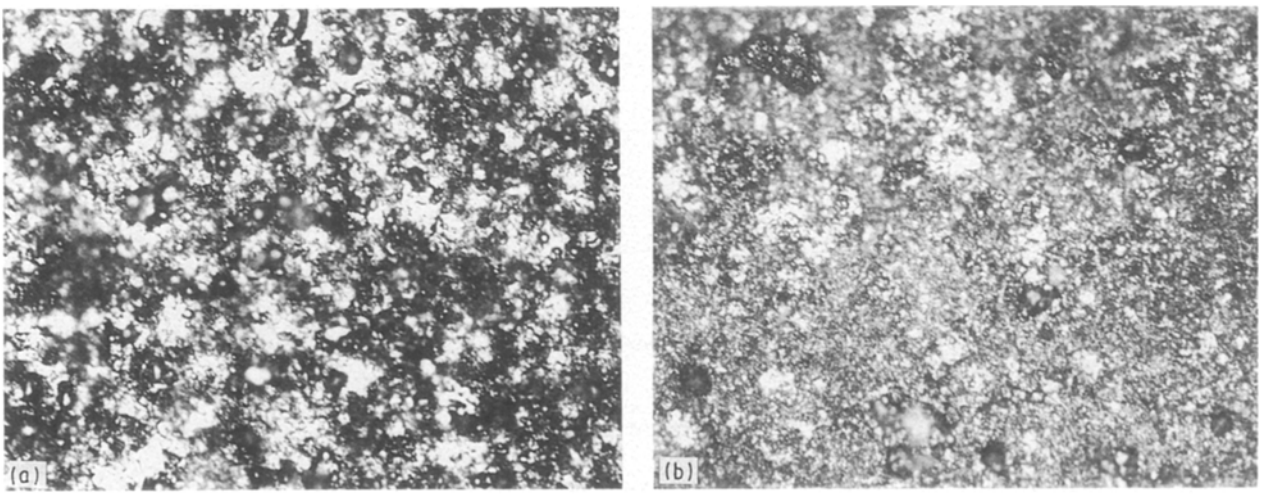

Figure 4 Optical micrograph of tantalum coating on WC–6Co substrate, × 200. (a) As-plasma-sprayed tantalum coating. (b) ROC processed at 1200 °C.

more dense and uniform, with a finer-grained appearance. Significantly fewer spherical particles (unmelted particles from the plasma-spray deposition process) were observed in the ROC-processed samples. It is apparent from these photomicrographs that ROC processing provides for significant morphological changes in the surface of the coatings, resulting in more uniform, denser coatings.

3.3. Erosive wear test results

Erosion testing was performed using a 30° angle of incidence and followed the ASTM standard. Testing was performed on three specimens: an uncoated substrate, a substrate with the as-sprayed tantalum coating, and an ROC-processed tantalum coated substrate. Two substrate materials were examined by erosion testing: WC–6Co and AlN. Representative test results are given in Table II (for the WC–6Co substrates) and Table III (for the AlN substrate).

The erosion-testing results for both substrates reveal that both the as-sprayed and ROC-processed coated samples exhibit *poorer* erosion resistance than the corresponding uncoated monolithic ceramic. For the as-sprayed tantalum metal coatings the dense, base ceramic would be expected to exhibit better erosion resistance than the porous as-sprayed metal coating. However, some improvement might have been expected if a dense, well-adhered ROC-produced tantalum carbide coating had been obtained. However, as the X-ray diffraction analysis discussed above revealed, ROC processing produced reactions between the deposited tantalum coating and the various sintering additives present in the ceramic substrates (and possibly the fluid die media used in the ROC process). These impurities would weaken the coating interface and probably the integrity of the coating itself. These results suggest that the influence of sintering additives, contained in ceramic substrates, in the conversion of applied metal coatings to ceramic coatings are detrimental to the performance of the ceramic coating. Such difficulties may also arise in other pressure-assisted densification methods (such as HIP) applied in an analogous manner.

4. Conclusions

In all cases the plasma-spray deposited tantalum coatings (present generally as $TaN_{0.1}$) were converted to tantalum carbide, TaC, after ROC processing at 1200 ° C. In addition, the presence of ATa_4O_{11} (where, for example, A = Ca) phases were observed in the post-ROC samples, suggesting that there is an interfacial reaction between the applied coating and sintering additives in the substrates.

Optical microscopy of the as-sprayed and post-ROC processed samples revealed that ROC processing eliminated many of the unmelted particulates present in the as-sprayed samples. In addition, treatment of the plasma-sprayed coatings via the high-pressure ROC process resulted in more dense and uniform coating morphologies.

Erosion testing pursuant to ASTM G65 was performed for the aluminium nitride and WC–Co substrates. Comparisons of erosion-resistance were made between the uncoated, as-sprayed, and post-ROC

TABLE II Representative 30° erosion data for uncoated, as-sprayed, and tantalum coated ROC-processed WC–6Co substrates, density 15.00

Sample	Time (min)	Weight (g)	Weight loss (g)	Cum. weight loss (g)
WC–6Co	0	157.2992		
78–43–4	5	157.2974	0.0018	0.0018
STB–824A	10	157.2876	0.0098	0.0116
	15	157.2852	0.0024	0.0140
	20	157.2830	0.0022	0.0162
	25	157.2819	0.0011	0.0155
	30	157.2798	0.0032	0.0194
	Volume	loss (mm^3)	1.2933	Total 0.0194
WC–6Co Ta	0	156.7580		
78–55–2	5	156.7544	0.0036	0.0036
LPPS Ta	10	156.7405	0.0139	0.0175
	15	156.7381	0.0024	0.0199
	20	156.7351	0.0030	0.0229
	25	156.7340	0.0011	0.0204
	30	156.7308	0.0043	0.0272
	Volume	loss (mm^3)	1.8133	Total 0.0272
WC–6Co Ta	0	157.5018		
ROC CUE2	5	157.4996	0.0022	0.0022
ROC processed	10	157.4860	0.0136	0.0158
Ta	15	157.4815	0.0045	0.0203
	20	157.4790	0.0025	0.0228
	25	157.4760	0.0030	0.0236
	30	157.4726	0.0064	0.0292
	Volume	loss (mm^3)	1.9467	Total 0.0292

TABLE III Representative 30° erosion data for uncoated, as-sprayed, and tantalum-coated ROC-processed AlN substrate, density 3.29

Sample	Time (min)	Weight (g)	Weight loss (g)	Cum. weight loss (g)
78-43-1	0	35.1402		
	5	35.1352	0.0050	0.0050
	10	35.1306	0.0046	0.0096
	15	35.1261	0.0045	0.0141
	20	35.1228	0.0033	0.0174
	25	35.1171	0.0057	0.0181
	30	35.1113	0.0115	0.0289
	Volume	loss (mm^3)	8.7842	Total 0.0289
78-43-16	0	36.4909		
LPPS Ta	5	36.4837	0.0072	0.0072
	10	36.4787	0.0050	0.0122
	15	36.4735	0.0052	0.0174
	20	36.4703	0.0032	0.0206
	25	36.4634	0.0069	0.0203
	30	36.4570	0.0133	0.0339
	Volume	loss (mm^3)	10.3040	Total 0.0339
ROC CUE2	0	36.4242		
ROC processed	5	36.4187	0.0055	0.0055
Ta	10	36.4142	0.0045	0.0100
	15	36.4103	0.0039	0.0139
	20	36.4051	0.0052	0.0191
	25	36.3991	0.0060	0.0196
	30	36.3947	0.0104	0.0295
	Volume	loss (mm^3)	8.9666	Total 0.0295

processed specimens. These results suggest that the presence of sintering additives in the substrates is detrimental to the performance of the metal-derived ceramic coating. Such difficulties may also arise in other pressure-assisted densification methods (such as HIP) applied in an analogous manner. Although variations in the ROC temperature may affect this reactivity of sintering aids, the temperature chosen for this study was sufficiently high that conversion of tantalum to TaC was ensured while still kept to a minimum, hopefully to reduce reactivity with the sintering additives.

Acknowledgements

K.E.H. wishes to acknowledge the assistance of Mr Bill Yates and Dr Walt Johnson of the Michigan Technological University; Ed Risk and Cliff Kelto, ROC Development Centre, Racheal Kent, Dow Central Research and Development – Advanced Ceramics Laboratory, Dr Bruce Peters and Dr Mike Paquette, Dow Discovery Research, for generous support of this project.

References

1. *Adv. Mater. Proc.* January (1991) 59.
2. D. APELIAN, *Int. J. Powder Metall.* **23** (1987) 249.
3. *Idem, Prog. Powder Metall.* **42** (1986) 17.
4. D. APELIAN, B. H. KEAR and H. W. SCHADLER, in "Rapidly Solidified Crystalline Alloys", edited by S. K. Das, B. H. Kear and C. M. Adam (The Metallurgical Society, Morristown, 1986).
5. P. MEYER and E. MUEHLBERGER, *Thin Solid Films* **98** (1984) 445.
6. H. B. v. NEDERVEEN, M. B. VERBURGH and J. M. HOUBEN, in "Proceedings of the 9th International Thermal Spraying Conference", May 1980, Nederlands Inst. voor Lastechnick, The Hague, pp. 256–62.
7. D. P. BUTT, J. J. MECHOLSKY Jr, M. v. ROODE and J. R. PRICE, *J. Amer. Ceram. Soc.* **73** (1990) 2690.
8. A. JOSHI, H. S. HU, L. JESION, J. J. STEPHENS and J. WADSWORTH, *Metall. Trans.* **21A** (1990) 2829.
9. C. A. KELTO, E. E. TIMM and A. J. PYZIK, *Ann. Rev. Mater. Sci.* **19** (1989) 527.
10. A. J. PYZIK, D. B. SCHWARZ, W. J. DUBENSKY and D. R. BEAMAN, U.S. Pat. 4919 689 (1990).
11. C. A. KELTO, Personal communication (1991).

Received 27 November 1991
and accepted 17 June 1992